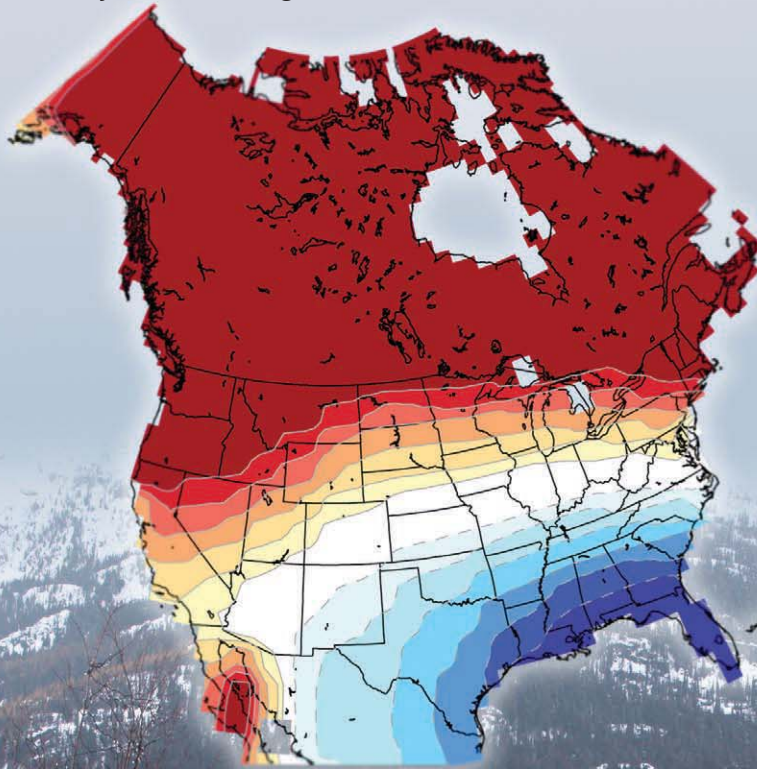


# STATE OF THE CLIMATE IN 2010

J. Blunden, D. S. Arndt, and M. O. Baringer, Eds.

Associate Eds. H. J. Diamond, A. J. Dolman, R. L. Fogt, B. D. Hall, M. Jeffries, J. M. Levy,  
J. M. Renwick, J. Richter-Menge, P. W. Thorne, L. A. Vincent, and K. M. Willett



**Special Supplement to the  
*Bulletin of the American Meteorological Society*  
Vol. 92, No. 6, June 2011**



## SIDEBAR 3.1: OCEAN SALINITY: A WATER CYCLE DIAGNOSTIC?—P. J. DURACK, S. E. WIJFFELS, AND N. L. BINDOFF

Present-day civilizations thrive in a wide range of temperatures at different latitudes across the Earth, but cannot cope without available freshwater. Changes to global water distribution are anticipated in the 21st century as anthropogenic climate change signatures become more apparent from natural variability of the climate system; future projections of surface moisture fluxes suggest that regions dominated by evaporation (over rainfall over the course of a year), will become drier, while regions dominated by rainfall (over evaporation) will become wetter (Allen and Ingram 2002; Held and Soden 2006; Meehl et al. 2007; Wentz et al. 2007; Seager et al. 2010). In water-stressed areas the human population and surrounding ecosystems are particularly vulnerable to decreasing or more variable rainfall due to climate change. Therefore, understanding probable future changes to the global water cycle are vital, as the projections of future climate show considerable changes to the water cycle are likely to significantly impact much of the world's population.

The global oceans cover 71% of the global surface, experience 75%–90% of global surface water fluxes, and contain 97% of the global freshwater volume (Schmitt 1995). As the ocean and land surface warms, so will the lower troposphere, and the amount of water vapor it can carry increases; this simple effect is anticipated to drive a stronger water cycle, with arid regions becoming drier and wet regions wetter (Held and Soden 2006). As the oceans are the engine room of the global water cycle, ocean salinity changes can be used to provide an estimate of broad-scale global water cycle changes and their regional patterns. Here, we review some of the major progress in understanding observed global water cycle changes in the ocean since the publication of the IPCC Fourth Assessment Report (AR4; Bindoff et al. 2007).

Global surface salinity is strongly correlated with the spatial patterns of E-P [evaporation (E) minus precipitation (P)] in the climatological mean. This relationship—where regions of low salinity correspond with regions of low (or negative) E-P and regions of high salinity with high E-P—provide some confidence in using salinity as a marker of global water cycle changes. Over long-timescales, the ocean inter-

grates and smoothes high frequency and spatially patchy E-P fluxes at the ocean surface and provides a smoothed salinity anomaly field that facilitates detection of large-scale changes.

Patterns of long-term changes to surface salinity are now available, based on both trend fits directly to ocean data (e.g., Freeland et al. 1997; Curry et al. 2003; Boyer et al. 2005; Gordon and Giulivi 2008; Durack and Wijffels 2010) and comparisons of Argo era (2003–present) modern- to historical-ocean climatologies (e.g., Johnson and Lyman 2007; Hosoda et al. 2009; Roemmich and Gilson 2009; von Schuckmann et al. 2009; Helm et al. 2010). The patterns of multidecadal salinity change from these analyses show remarkable similarities between the mean E-P field and mean salinity field (Fig. 3.17). Rainfall-dominated regions such as the western Pacific warm pool, for example, have undergone a long-term freshening, and arid regions in the subtropical, evaporation-dominated ‘desert latitudes’ have generally increased in salinity (e.g., Fig. 3.17b).

Observed surface salinity changes suggest that changes in the global water cycle have occurred. The mean surface salinity climatology and the pattern of multidecadal (50-year) linear surface salinity changes (Durack and Wijffels 2010) have a spatial correlation of 0.7 (Fig. 3.18). Using this spatial relationship the amount of salinity pattern amplification can be obtained, with these data implying an amplification of the mean ocean surface salinity pattern of 8.0% has occurred between 1950 and 2000 (Fig. 3.18). In order to enhance the signal-to-noise for pattern

*Continues on next page*

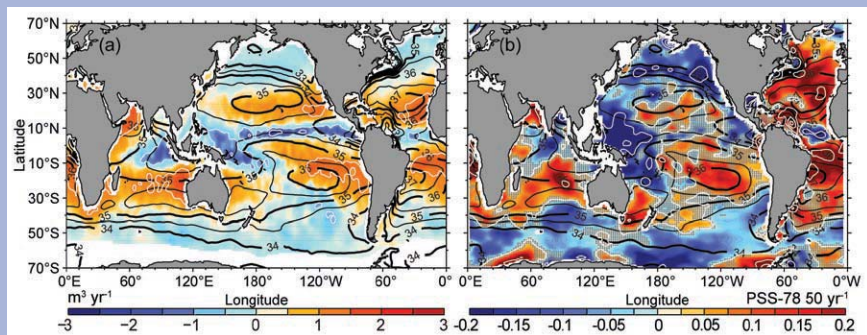


**FIG. 3.17.** (a) Ocean-atmosphere freshwater flux (E-P;  $\text{m}^3 \text{yr}^{-1}$ ) averaged over 1980–93 (Josey et al. 1998). Contours every  $1 \text{ m}^3 \text{yr}^{-1}$  in white. (b) The 50-year linear surface salinity trend (PSS-78  $50 \text{ yr}^{-1}$ ). Contours every 0.25 (PSS-78) are plotted in white. On both panels, the 1975 surface mean salinity is contoured black [contour interval 0.5 (PSS-78) for thin lines, 1 for thick lines]. Due to limited observational E-P coverage a direct 1950–2000 climatology is not currently available, however the field produced by Josey et al. 1998 closely matches climatological means developed from many varied products over differing time periods (e.g. da Silva et al. 1994; Schanze et al. 2010) and provide a very similar spatial E-P pattern of correspondence with surface climatological mean salinity. Reproduced from Durack and Wijffels (2010).

cont. **SIDEBAR 3.1: OCEAN SALINITY: A WATER CYCLE DIAGNOSTIC?—**  
P. J. DURACK, S. E. WIJFFELS, AND N. L. BINDOFF

amplification a spatial smoothing technique is applied to the global data; this develops basin-bound zonal means for both climatological mean salinity anomalies (compared with the global surface climatological mean salinity) and their associated 50-year salinity trends, and are termed basin-zonally-averaged means and anomalies, respectively. This robust global tendency towards an enhanced surface salinity pattern provides broad-scale agreement with the regional studies of Cravatte et al. (2009) and Curry et al. (2003), and numerous global analyses of surface salinity change (e.g., Boyer et al. 2005; Hosoda et al. 2009; Roemmich and Gilson 2009). These ocean surface salinity changes demonstrate that wet regions get fresher and dry regions saltier, following the expected response of an amplified water cycle.

Patterns of long-term subsurface salinity changes on pressure surfaces also largely follow an enhancement of the existing mean pattern. The interbasin contrast between the Atlantic (salty) and Pacific (fresh) intensifies over the observed record (e.g., Boyer et al. 2005; Johnson and Lyman 2007; Gordon and Giulivi 2008; Hosoda et al. 2009; Roemmich and Gilson 2009; von Schuckmann et al. 2009; Durack and Wijffels 2010). These deep-reaching salinity changes suggest that past water cycle changes have propagated into the ocean interior, with a clear enhancement to the high-salinity subtropical waters, and freshening of the high-latitude waters. A particularly strong and coherent freshening expressed in the Antarctic intermediate water subduction pathway centered around 50°S has also been detected (Johnson and Orsi 1997; Wong et al. 1999; Bindoff and McDougall 2000; Antonov et al. 2002; Curry et al. 2003;

freshening has occurred in the upper 100 m. A region of salinification occurs centered at 48°N. Freshening occurs in the 30°N–45°N belt extending to 1000 m depth. Salinification occurs in the upper 50 m of the 10°N–30°N belt. At 12°N, freshening occurs centered about a depth of 100 m. A belt of salinification occurs centered at 20°N between 150 m and 800 m depth. In the 0°–10°S, belt there is a region of relatively large salinification limited to approximately the upper 50 m. In the 10°S–20°S region, there is salinification suggesting an increase in SMW production or an increase in its salinity. In the region 25°S–30°S, freshening has occurred. Centered at 40°S, salinification has occurred in the 125 m–700 m layer.

g. *Surface currents*—R. Lumpkin, K. Dohan, and G. Goni

Near-surface currents are measured in situ by drogued satellite-tracked drifting buoys and by current meters on moored Autonomous Temperature

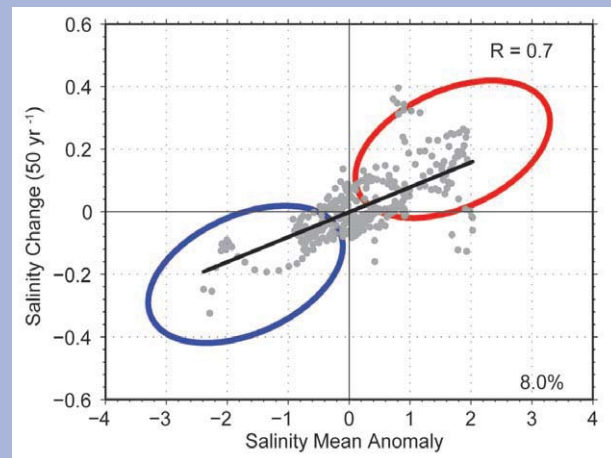


**FIG. 3.18. Observed surface salinity changes versus mean salinity anomalies—fresh gets fresher and salty waters saltier. The x-axis is the basin zonally-averaged anomaly from the mean surface salinity (34.8 PSS-78), and the y-axis is the associated basin zonally-averaged multidecadal linear salinity change trend (PSS-78 50 yr<sup>-1</sup>). The blue and red ellipses are representative of regions where fresh (compared to the global surface mean salinity) are getting fresher and salty getting saltier, respectively. Using the full global surface salinity analysis (Durack and Wijffels 2010), and basin-zonal mean averaging to enhance the signal-to-noise, yields a mean salinity climatology pattern amplification of 8%.**

Line Acquisition System (ATLAS) buoys.<sup>1</sup> During 2010, the drifter array ranged in size from a minimum of 887 drogued buoys to a maximum of 1184, with a median size of 1129 drogued buoys (undrogued drifters continue to measure SST, but are subject to significant wind slippage; Niiler et al. 1987). The moored array included 37 buoys with current meters, all between 12°S and 21°N. These tropical moorings compose the TAO/TRITON (Pacific; 16 buoys with current meters), PIRATA (Atlantic; 6 buoys) and RAMA (Indian; 15 buoys) arrays.

<sup>1</sup> Drifter data is distributed by NOAA/AOML at <http://www.aoml.noaa.gov/phod/dac/gdp.html>. Moored data is distributed by NOAA/PMEL at <http://www.pmel.noaa.gov/tao>. OSCAR gridded currents are available at <http://www.oscar.noaa.gov/> and <http://podaac.jpl.nasa.gov/>. AVISO gridded altimetry is produced by SSALTO/DUACS and distributed with support from CNES, at <http://www.aviso.oceanobs.com/>. Analyses of altimetry-derived surface currents are available at <http://www.aoml.noaa.gov/phod/altimetry/cvar>.

Boyer et al. 2005; Roemmich and Gilson 2009; Hosoda et al. 2009; Durack and Wijffels 2010; Helm et al. 2010). Studies have also reported long-term and coherent salinity changes on subsurface density horizons (e.g., Wong et al. 1999; Curry et al. 2003; Helm et al. 2010). In this framework Durack and Wijffels (2010), show that many changes are dominated by subduction into the deep ocean driven by a broad-scale warming, and thus are less useful in reflecting changes in the water cycle.

In summary, several recent studies employing different analysis techniques find a clear multidecadal ocean surface salinity change. Broad-scale changes can be characterized as an amplification of the climatological salinity pattern, a tendency also found in the subsurface. The consensus view of coherent salinity change arises, even though many different analysis techniques and ocean salinity observing platforms have been used—reflecting the robustness of the signal. To first order, this suggests that broad zonal changes to E-P have changed ocean surface salinity, and changes are propagating into the subsurface ocean following the mean circulation pathways. An enhancement to mean salinity patterns and basin contrasts are the result.

How rates of salinity changes translate into rates of water cycle change remains to be determined. The ocean mixing through circulation and subduction of salinity anomalies reduces the E-P surface flux changes expressed in surface ocean salinity. Global coupled ocean-atmosphere climate models are the best tools currently available to investigate salinity and E-P

change relationships, as the current observed record is too temporally and spatially sparse.

Many previous studies have used regional and global estimates of ocean salinity changes to infer water cycle changes. Hosoda et al. (2009) presented estimates of water cycle enhancement, derived from ocean salinity change trends by comparing the Argo period (2003–07) against the World Ocean Database (~1960–89). They reported an inferred global E-P enhancement of  $3.7 \pm 4.6\%$  over their 30-year comparison, which considered surface salinity layer changes to 100 m depth. This enhancement is supported by the results of Trenberth et al. (2007) and Yu (2007), obtained from correlations with SST 1970–2005 (4%) and evaporation estimates 1978–2005 (~10%) respectively.

This ocean footprint of a strengthening water cycle captured in surface (and subsurface) salinity changes suggests that the remaining 29% of the global terrestrial surface has also likely experienced changes over the 1950–2000 period. Continued monitoring of future ocean property changes are necessary to effectively monitor and diagnose the effect of anthropogenic change and the rate of its evolution on our global climate system.

For homogeneous coverage and analyses such as the one presented here, ocean currents are estimated using two methodologies, both using the Archiving, Validation and Interpretation of Satellite Oceanographic data (AVISO) multimission altimeter near-real time gridded product. The first is a synthesis of AVISO with in situ drifter measurements and reanalysis winds (Niiler et al. 2003), which adjusts the altimeter-derived geostrophic velocity anomalies to match the observed in situ eddy kinetic energy. The second is the purely satellite-based OSCAR (Ocean Surface Current Analyses–Real time) product, which uses AVISO altimetry, winds, SST, and the Rio05 mean dynamic topography (Rio and Hernandez 2004) to create a  $0.33^\circ$ -resolution surface current maps averaged over the 0 m–30 m layer of the ocean (Bonjean and Lagerloef 2002). In both cases, anomalies are calculated with respect to the time period 1992–2007.

Global zonal current anomalies, and changes in

anomalies from 2009, are shown in Figs. 3.19 and 3.20 and discussed below for individual ocean basins. In the analysis, an “eastward anomaly” is an increase in an eastward current, or a decrease in a westward current, and indicated as a positive zonal current anomaly. Similarly, negative anomalies are westward (decrease in an eastward current, or increase in a westward one).

#### 1) PACIFIC OCEAN

In the equatorial Pacific, 2010 began with equatorial eastward anomalies of  $\sim 50 \text{ cm s}^{-1}$  in the center and western side of the basin, associated with the El Niño event of 2009 (Fig. 3.20). By the end of January, eastward anomalies persisted west of the dateline, but strong ( $30 \text{ cm s}^{-1}$ – $50 \text{ cm s}^{-1}$ ) westward anomalies had developed in the longitude band  $130^\circ\text{W}$ – $160^\circ\text{W}$ . The region of eastward anomalies propagated east across the Pacific during February through early March, while westward anomalies grew in their wake. By

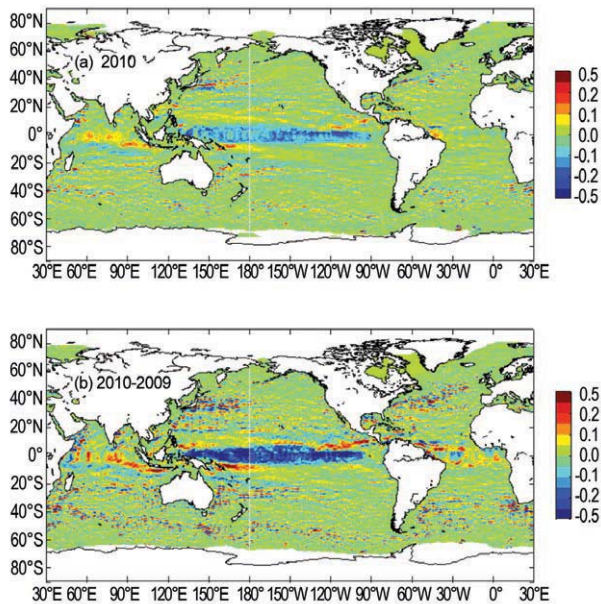


**FIG. 3.19. Global zonal geostrophic anomalies for 2010 (top) and 2010 minus 2009 (bottom),  $\text{cm s}^{-1}$ , derived from a synthesis of drifters, altimetry, and winds.**

April, westward anomalies were found across the entire equatorial Pacific. These anomalies reached their maximum amplitudes in mid-to-late May, with values of  $60 \text{ cm s}^{-1}$ – $70 \text{ cm s}^{-1}$  in the longitude band  $110^\circ\text{W}$ – $140^\circ\text{W}$ . This La Niña pattern persisted through boreal summer, although its amplitude diminished through this time period. The anomalous westward advection of salty water likely contributed to salty surface anomalies in the western equatorial Pacific (Fig. 3.12b). By October, the westward anomaly pattern was sufficiently weak that mesoscale patterns associated

with tropical instability waves began dominating the surface current anomaly field in the region.

Surface current anomalies in the equatorial Pacific typically lead SST anomalies by several months, with a magnitude that scales with the SST anomaly magnitude. Recovery to normal current conditions is also typically seen before SST returns to normal. Thus, current anomalies in this region are a valuable predictor of the evolution of SST anomalies and their related climate impacts. This leading nature can be seen clearly in the first principal empirical orthogonal function (EOF) of surface current anomaly and separately of SST anomaly in the tropical Pacific basin (Fig. 3.20). In mid-2010, the values of the normalized surface current and SST EOFs exceeded those of the 2000 and 2008 La Niñas, and hence by this metric, this year’s La Niña was the strongest such event in the last decade.

In 2010, the Kuroshio Current exhibited a more stable path than in the last several years, with a narrower and stronger annual mean signature and a reduced area of enhanced eddy kinetic energy. Compared to 2006–09, the Kuroshio shifted approximately  $1^\circ$  in latitude to the north (Fig. 3.21). This shift may be related to the Kuroshio extension jet entering the strong phase of a decadal-scale fluctuation associated with the strength of the Kuroshio recirculation gyre and stability of the jet (Qiu and Chen 2005). Qiu and Chen (2005) hypothesized that this fluctuation is driven by the Pacific Decadal Oscillation (PDO), which in its negative (positive) phase generates negative (positive) sea height anomalies in the northeast Pacific which propagate to the western boundary and weaken (strengthen) the Kuroshio jet. Possibly consistent with this hypothesis, the PDO index generally dropped from 2004 to 2008 but rapidly increased through the latter part of 2009 and early 2010 (Yu and Weller 2010). However, it subsequently dropped precipitously in July 2010 (see the “Monthly Ocean Briefing” presentation by NOAA’s Climate Prediction Center at <http://www.cpc.ncep.noaa.gov/products/GODAS>), suggesting that the northward shift may not persist through 2011.

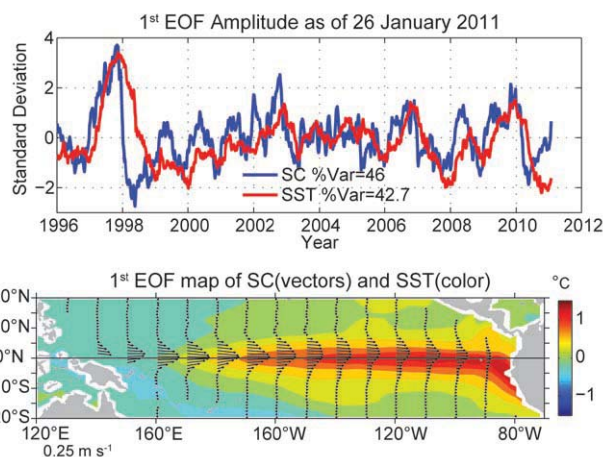


**FIG. 3.20. Principal empirical orthogonal functions (EOF) of surface current (SC) and of SST anomaly variations in the tropical Pacific from the OSCAR model. Top: Amplitude time series of the EOFs normalized by their respective standard deviations. Bottom: Spatial structures of the EOFs.**

## 2) INDIAN OCEAN

Westward equatorial anomalies began developing in the western Indian Ocean in January, and by mid-February exceeded  $50 \text{ cm s}^{-1}$  at  $50^\circ\text{E}$ – $65^\circ\text{E}$ , with weaker westward anomalies from  $80^\circ\text{E}$  to the West African coast. This short-lived anomaly pattern was gone by the end of March. In July, weaker eastward anomalies began developing in the center and eastern side of the